

Undersampled MRI Reconstruction with Side Information-Guided Normalisation

Xinwen Liu¹, Jing Wang², Cheng Peng³, Shekhar S. Chandra¹, Feng Liu¹, and S. Kevin Zhou^{4,5}

¹ School of Information Technology and Electrical Engineering,
The University of Queensland, Brisbane, Australia.

² The Commonwealth Scientific and Industrial Research Organisation,
Canberra, Australia.

³ Johns Hopkins University, Baltimore, USA.

⁴ School of Biomedical Engineering & Suzhou Institute for Advanced Research
Center for Medical Imaging, Robotics, and Analytic Computing & LEarning
(MIRACLE), University of Science and Technology of China, Suzhou, 215123, China.

⁵ Key Lab of Intelligent Information Processing of Chinese Academy of Sciences
(CAS), Institute of Computing Technology, CAS, Beijing, 100190, China.

Abstract. Magnetic resonance (MR) images exhibit various contrasts and appearances based on factors such as different acquisition protocols, views, manufacturers, scanning parameters, etc. This generally accessible appearance-related side information affects deep learning-based undersampled magnetic resonance imaging (MRI) reconstruction frameworks, but has been overlooked in the majority of current works. In this paper, we investigate the use of such side information as normalisation parameters in a convolutional neural network (CNN) to improve undersampled MRI reconstruction. Specifically, a **Side Information-Guided Normalisation (SIGN)** module, containing only few layers, is proposed to efficiently encode the side information and output the normalisation parameters. We examine the effectiveness of such a module on two popular reconstruction architectures, D5C5 and OUCR. The experimental results on both brain and knee images under various acceleration rates demonstrate that the proposed method improves on its corresponding baseline architectures with a significant margin.

Keywords: Deep Learning · Undersampled MRI Reconstruction

1 Introduction

Magnetic resonance imaging (MRI) is a non-invasive imaging modality that produces high contrast in vivo imaging of soft-tissue with non-ionizing radiation. However, due to hardware constraints, MRI suffers from a long scanning time, which impedes its application to real-time imaging. Undersampling the measurements is a common approach that accelerates the imaging process, but can result in blurriness and artifacts that are not suitable for diagnosis purposes.

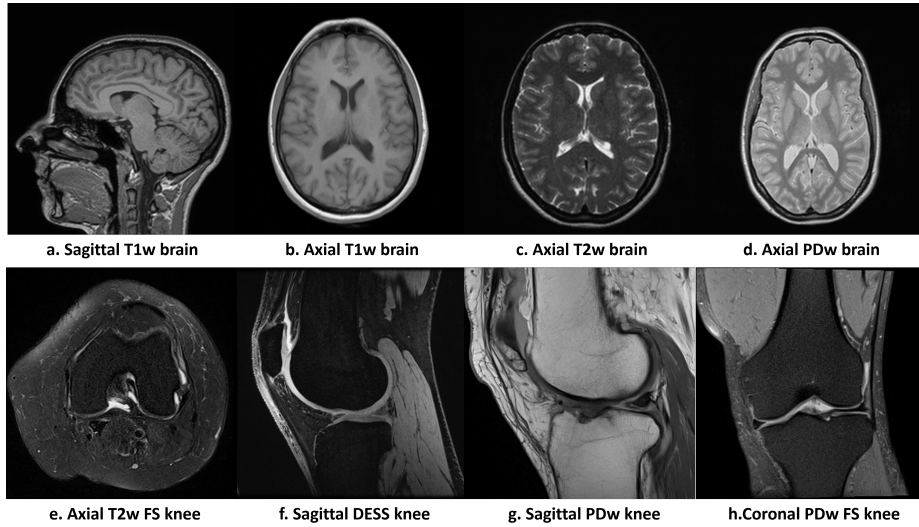


Fig. 1. MR images of various views, anatomies and acquisition protocols acquired on different machines. a and d are from IXI database; b, c, e, g and h are from fastMRI database [15,28]; and f is from SKM-TEA database [3].

Deep learning (DL) has been widely studied to reconstruct the high-quality images from the undersampled measurements [2,7,14,20,32]. Initially, convolutional neural networks (CNN) have been employed [10,24,26] to directly map the undersampled images or measurements to fully-sampled ones. Later, imaging model has been integrated into the learning pipeline, and model-based learning has achieved the state-of-the-art performance [1,9,13,18,19,21,22,23,26,27,30]. More recently, transformers have been integrated into the CNN-based networks for MRI undersampled reconstruction [4,6,16,29]. These networks can reconstruct MR images with a high fidelity.

MR images present various appearances based on different acquisition protocols, imaging views, scanning parameters, manufacturers, etc. Fig. 1 shows examples of MR images with diverse appearances. When comparing b,c and d, we can observe that for axial brain images, varying acquisition protocols results in differences in brightness, contrast and saturation. This image style variations with acquisition protocols can also be observed by comparing f and g. In addition, due to the hardware differences, images acquired on different machines with divergent scanning parameters present variant noise levels and resolutions. The same subject with different views also shows dissimilar structures. All these differences during acquisitions result in different image styles, which can affect the performance of undersampled reconstruction algorithms [8,17,25,31].

Based on such an observation and inspired by recent works on style-related normalisation [5,11,12,17], we propose a **Side Information-Guided Normalisation**

(SIGN) module that can be inserted in CNN-based reconstruction networks to obtain higher quality reconstructed image. Specifically, the SIGN module is a sub-network that contains a few linear, normalisation, and non-linear layers. We leverage the side information, which is commonly accessible, and encode it in the SIGN module. SIGN’s outputs are used to normalise the feature maps generated by the reconstruction backbone. In this study, we inserted the SIGN modules into the popular D5C5 [21] and OUCR [7] backbones. The experiments on brain and knee images under $4\times$ and $6\times$ acceleration show that these networks can obtain significantly better performances by including SIGN modules.

2 Methods

2.1 Problem formulation

Reconstructing an image $\mathbf{x} \in \mathbb{C}^N$ from undersampled measurement $\mathbf{y} \in \mathbb{C}^M$ ($M \ll N$) with side information is formulated as an inverse problem [21,32]:

$$\min_{\mathbf{x}} \mathcal{R}(\mathbf{x}, \mathbf{s}) + \lambda \|\mathbf{y} - \mathbf{F}_u \mathbf{x}\|_2^2, \quad (1)$$

where $\mathbf{s} = [\mathbf{s}_e, \mathbf{s}_c]$ represents the side information encoded as input vectors to the model, \mathcal{R} is the regularisation term on \mathbf{x} and \mathbf{s} , $\lambda \in \mathbb{R}$ denotes the balancing coefficient between \mathcal{R} and data consistency (DC) term, $\mathbf{F}_u \in \mathbb{C}^{M \times N}$ is an undersampled Fourier encoding matrix. In model-based learning, Eq. (1) is incorporated in the network architecture with \mathcal{R} approximated by the convolution and linear layers.

We divide the side information into two types: categorical variables $\mathbf{s}_e = (s_e^1, s_e^2, \dots, s_e^{n_1})$ and continuous variables $\mathbf{s}_c = (s_c^1, s_c^2, \dots, s_c^{n_2})$ based on the specific piece of information. For attributes such as views, acquisition protocols and manufacturers, they are in distinct groups with a finite number of categories. We use embedding vectors to represent each of these categorical variables. The scanning parameters, such as repetition time (TR), echo time (TR) and flip angles, are continuous variables, which are stacked as vectors. Formally, for each categorical variable $s_e^i, i = 1, 2, \dots, n_1$, we can obtain the embedded vector \mathbf{V}_e^i as:

$$\mathbf{V}_e^i = \text{Embedding}(s_e^i). \quad (2)$$

For the continuous variables \mathbf{s}_c , we have:

$$\mathbf{V}_c = \mathbf{W} \mathbf{s}_c + \mathbf{b}, \quad (3)$$

where \mathbf{V}_c is the representation of continuous information, and \mathbf{W} and \mathbf{b} are parameters of the linear mapping layer.

2.2 Side Information-Guided Normalisation (SIGN) module

To integrate the side information into a network and interact with the main reconstruction network, we propose a Side Information-Guided Normalisation

(SIGN) module. Fig. 2 shows the architecture of the proposed SIGN module, which contains linear layers, non-linear activation function (ReLU) and layer normalisation (LN). The inputs to the SIGN module are the side information and the outputs are the parameters to be fed into the reconstruction backbone.

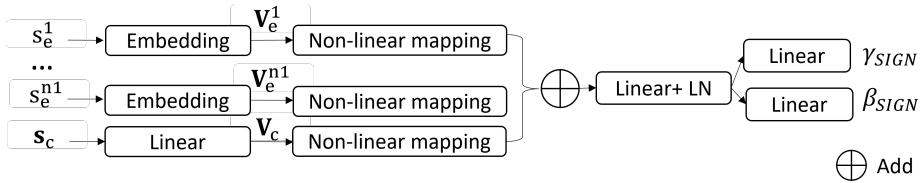


Fig. 2. The architecture of Side Information-Guided Normalisation (SIGN) module. The inputs are the side information, and the outputs are the parameters to interact with the reconstruction backbone.

First, the side information \mathbf{s} is encoded into vectors $\{\mathbf{V}_e^i\}$ and \mathbf{V}_c . Then, these vectors are passed through the non-linear mapping blocks in parallel. Each of these blocks comprise a fully-connected layer, LN, and ReLU. The latent individual side information features are merged together by element-wise additive operation. At the end, the merged features are fed into another fully-connected layers to further model relationships among each piece of side information. The output parameters γ_{SIGN} and β_{SIGN} are sent into the reconstruction backbone.

Motivated by [5,11,12,17], the changes of contrasts and texture distributions in images can be mainly described by the mean and variance of feature maps in a deep CNN. Thus, we propagate the encoded side information to control the mean and standard deviation of each feature map in the reconstruction backbone. Note before applying the affine parameters on each layer, we normalize the feature maps per instance to a zero mean and a unit standard deviation. Since different layers have different feature distributions, the SIGN module is not shared cross layers. Formally, for layer l with feature map h_l in the reconstruction backbone:

$$\text{SIGN}(h_l) = \gamma_{SIGN}^l \left(\frac{h_l - \mu(h_l)}{\sigma(h_l)} \right) + \beta_{SIGN}^l, \quad (4)$$

where γ_{SIGN}^l and β_{SIGN}^l are the outputs of the SIGN module, and $\mu(h_l)$ and $\sigma(h_l)$ are the mean and standard deviation of the feature map, respectively, computed across spatial dimensions ($H \times W$) independently for each channel.

2.3 Reconstruction with D5C5 and OUCR backbones

D5C5 [21] and OUCR [7] are high performance backbones for undersampled MRI reconstruction. D5C5 is a deep cascaded network that contains five interleaved CNN blocks and data consistency (DC) layers. In each of the CNN block,

there are five convolutional layers with ReLU activation function and a residual connection at the end. As shown in Fig. 3, we insert the SIGN modules into the CNN blocks after each of the convolutional layers, except the last one.

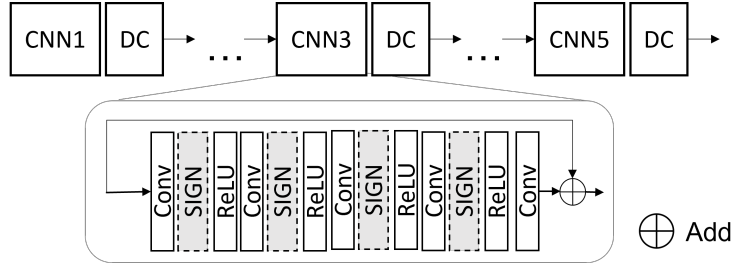


Fig. 3. The D5C5 reconstruction architecture with the SIGN modules inserted after convolution layers.

OUCR is a convolutional recurrent neural network (CRNN) that contains the over complete CRNN (OC-CRNN), the under complete CRNN (UC-CRNN) and a refine module, as shown in Fig. 4. The encoder in UC-CRNN uses maxpooling to reduce the feature map size before being fed into the residual block and the decoder which upsamples the feature map to the original size. The OC-CRNN enlarges the feature map size in the encoder with the upsampling operations. The enlarged feature maps are fed into the residual block and the decoder where the feature maps is down-sampled to the original size. Both OC-CNN and UC-CNN contain an ordinary residual block of convolutions with a skip connection. At the end of the network, a refine block with stacked convolutional layers and ReLU activation functions refine and output the reconstructed results. More details of OUCR can be found in [7]. The SIGN modules are inserted after each convolutional layer, except the last convolutional layers in the decoder and refine module, which are used to reserve varied feature maps. The numbers of hidden nodes in the fully-connected layers of SIGN modules are assigned to be the same as the number of feature maps in the corresponding layers, except the one in the linear layer after add operation, which is double of the feature map numbers.

The networks are trained with a mean-absolute-error loss. First, we pretrain the backbone and SIGN modules together. To better optimise the networks, we fix the parameters of the convolutional layers, and only fine-tune the parameters of the linear layers in SIGN modules.

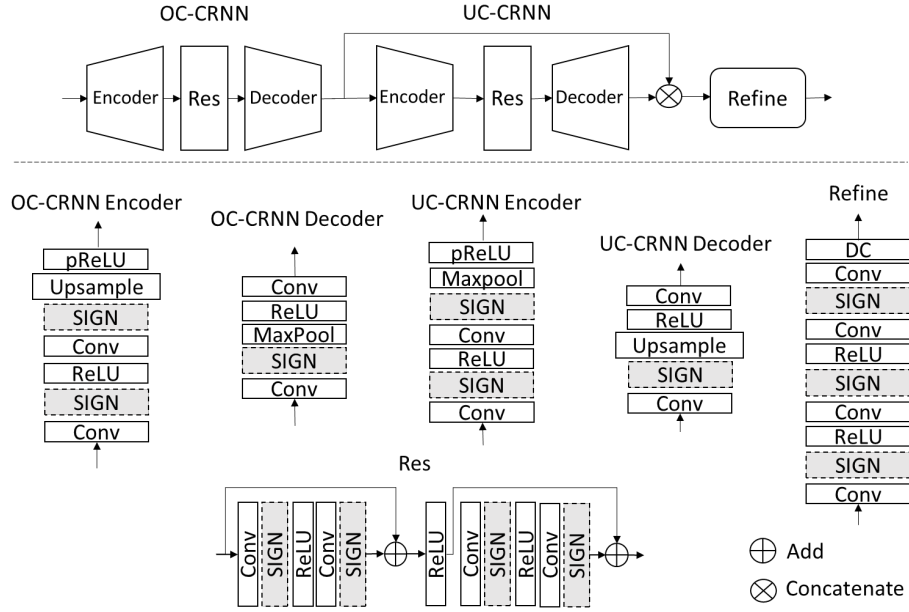


Fig. 4. The OUCR reconstruction architecture with the SIGN model inserted after convolution layers.

3 Experiments and results

3.1 Datasets and network configuration

We evaluate the proposed method on both brain and knee datasets. The brain dataset contains DICOM images from the NYU fastMRI⁶ database [15,28] and IXI database⁷. The side information in the brain dataset include contrast (T1-weighted, T2-weighted, proton-density-weighted, and magnetic resonance angiogram), views (axial and sagittal), source (Siemens, Philip and GE), and scanning parameters (repetition time, echo time and flip angle). The knee dataset is comprised of DICOM images from the NYU fastMRI database and SKM-TEA database[3]. The side information in the knee dataset contains contrast (T2-weighted fat saturated, proton-density-weighted, proton-density-weighted fat saturated, and double echo steady state) and views (axial, sagittal and coronal) and scanning parameters (repetition time, echo time and flip angle). It is noted that for IXI database, the scanning parameters are unknown, so we code it as zeros, and the images are indistinguishable from the manufacturers, so we code it as unknown source. In total, there are 10,534 brain slices from 437 volumes and

⁶ fastmri.med.nyu.edu

⁷ <https://brain-development.org/ixi-dataset/>

11,406 knee slices from 246 volumes. For each dataset, 80% of the volumes are randomly extracted for training, 10% for validation, and 10% for testing.

For this experiment, all the data are emulated single-coil magnitude-only images. We crop and resize the images into 320×320 and retrospectively undersampled the Cartesian k -space with 1D Gaussian sampling pattern. The evaluation is conducted under acceleration rates of $4\times$ and $6\times$ using structural similarity index (SSIM) and peak signal-to-noise ratio (PSNR) as performance metrics. We calculate and report the mean value of the metrics for reconstructed test images.

The experiments are carried out on NVIDIA SXM-2 Tesla V100 Accelerator Units. The networks are implemented on Pytorch and trained using the Adam optimizer with a weight decay to prevent over-fitting.

3.2 Results

The quantitative comparison of the proposed method and baseline models is shown in Table 1. The first row shows the metrics of the undersampled images reconstructed directly from the zero-filled k -space. D5C5 (row 2) and OUCR (row 4) both improve the PSNR and SSIM over the undersampled images, with OUCR outperforming D5C5 on all cases, which is consistent with [7]. Comparing D5C5 and D5C5+SIGN, the proposed design improves PSNR by about 2–2.5dB on brain images, and 1.5dB on knee images. The improvements are also observed on SSIM, with about 1.5% and 2% on brain and knee images, respectively. For the experiments on OUCR backbone, the performances of OUCR+SIGN are consistently better than those of OUCR. Overall, the experiments show that the simple and effective design of SIGN improves the baseline model with a considerable margin. OUCR+SIGN performs slightly lower than D5C5+SIGN. The reason could be due to the complexity of OUCR. Different from D5C5 which has a unified straightforward architecture, OUCR has recurrent designs, multiple residual connections, and varying sizes of feature maps [7]. More careful consideration in inserting SIGN module has the potential to improve the results but is out of the scope of this paper.

Table 1. Quantitative comparison on the reconstruction of brain and knee images under acceleration rates of $4\times$ and $6\times$.

	4 \times				6 \times			
	PSNR(dB)		SSIM(%)		PSNR(dB)		SSIM(%)	
	Brain	Knee	Brain	Knee	Brain	Knee	Brain	Knee
Undersampled	29.92	30.04	79.27	79.16	22.03	24.63	60.02	66.49
D5C5	39.29	35.34	96.89	90.69	36.03	33.23	94.62	87.51
D5C5+SIGN	41.70	37.18	97.93	93.02	38.16	34.66	96.39	89.75
OUCR	40.29	36.48	97.44	92.29	36.93	34.16	95.58	89.17
OUCR+SIGN	41.64	37.06	97.94	92.93	37.96	34.47	96.27	89.51

Fig. 5 shows the examples of reconstructed brain images under $4\times$ acceleration with different methods. The first column is the fully-sampled images and the second column represents the undersampled images, which are blurry and full of artifacts. As shown in the third column, D5C5 can reconstruct the images. In the fourth column, D5C5+SIGN further improves the images with more detailed information preserved, as pointed by the arrows. Similar trend can also be observed by comparing the fifth column (OUCR) and the sixth column (OUCR+SIGN). OUCR with the SIGN inserted in the network recovers the images with higher visual fidelity.

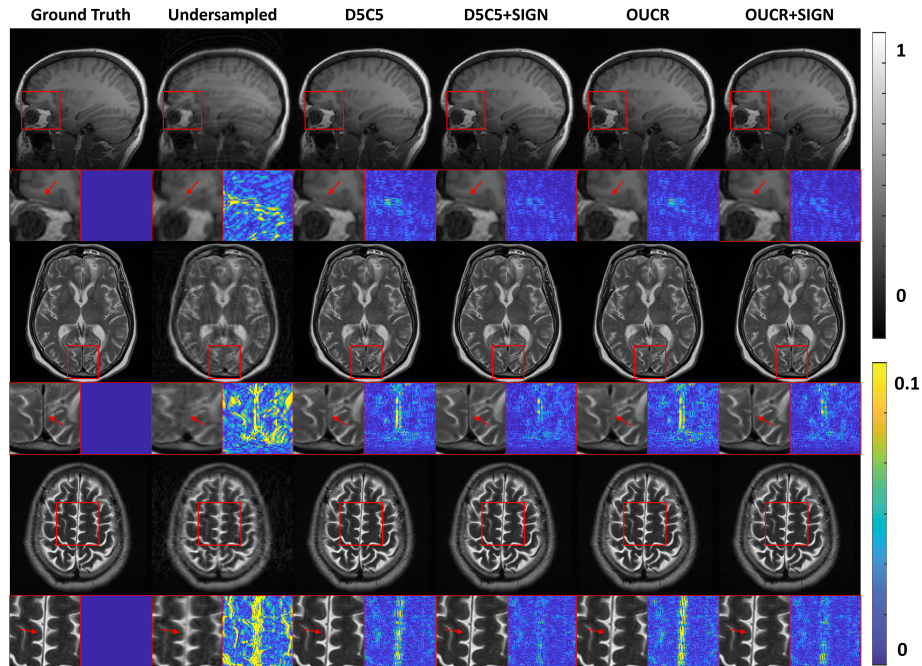


Fig. 5. The reconstructed brain images under $4\times$ acceleration with different methods.

3.3 Further analysis

This section further investigates the effectiveness of the proposed SIGN module. As an example, we test the D5C5+SIGN model in recovering $4\times$ accelerated brain images. In the first experiment, we set the side information of each image with a random label. The results show that the PSNR drops from 41.70dB to 40.93dB. Then, we evaluate the reconstruction with wrong side information. For example, for the image with axial view, we assign it to be the sagittal view. The performance drops by approximately 1dB.

In addition, the importance of each side information is evaluated by masking out one or more branch of the side information in SIGN. When only using the contrast information, the performance goes down to 41.39dB. With view information alone, PSNR is 40.94dB. If both contrast and view information are used, PSNR becomes 41.42dB. More comparison and results can be found in the supplementary material (Table S1-2). Overall, reconstructing images with wrong or missing side information leads to a worse performance.

4 Conclusion

In this paper, we propose to utilise the side information as normalisation parameters to improve the undersampled MRI reconstruction. Experimental results demonstrate the proposed approach can improve the baseline models significantly on both brain and knee images under $4\times$ and $6\times$ acceleration. While the current design is based on the popular D5C5 and OUCR architectures, the proposed framework is extendable to other network architectures. The current study is based on the single-coil magnitude-only images for proof-of-concept. In the future, we will adapt the network to multi-coil complex-valued datasets.

References

1. Aggarwal, H.K., Mani, M.P., Jacob, M.: MoDL: Model-based deep learning architecture for inverse problems. *IEEE transactions on medical imaging* **38**(2), 394–405 (2018)
2. Chandra, S.S., Bran Lorenzana, M., Liu, X., Liu, S., Bollmann, S., Crozier, S.: Deep learning in magnetic resonance image reconstruction. *Journal of Medical Imaging and Radiation Oncology* **65**(5), 564–577 (2021)
3. Desai, A.D., Schmidt, A.M., Rubin, E.B., Sandino, C.M., Black, M.S., Mazzoli, V., et al.: Skm-tea: A dataset for accelerated mri reconstruction with dense image labels for quantitative clinical evaluation. In: *Thirty-fifth Conference on Neural Information Processing Systems Datasets and Benchmarks Track (Round 2)* (2021)
4. Feng, C.M., Yan, Y., Fu, H., Chen, L., Xu, Y.: Task transformer network for joint mri reconstruction and super-resolution. In: *International Conference on Medical Image Computing and Computer-Assisted Intervention*. pp. 307–317. Springer (2021)
5. Gu, J., Ye, J.C.: Adain-based tunable cyclegan for efficient unsupervised low-dose ct denoising. *IEEE Transactions on Computational Imaging* **7**, 73–85 (2021)
6. Guo, P., Mei, Y., Zhou, J., Jiang, S., Patel, V.M.: Reconformer: Accelerated mri reconstruction using recurrent transformer. *arXiv preprint arXiv:2201.09376* (2022)
7. Guo, P., Valanarasu, J.M.J., Wang, P., Zhou, J., Jiang, S., Patel, V.M.: Over-and-under complete convolutional rnn for mri reconstruction. In: *International Conference on Medical Image Computing and Computer-Assisted Intervention*. pp. 13–23. Springer (2021)
8. Guo, P., Wang, P., Zhou, J., Jiang, S., Patel, V.M.: Multi-institutional collaborations for improving deep learning-based magnetic resonance image reconstruction using federated learning. In: *Proceedings of the IEEE/CVF Conference on Computer Vision and Pattern Recognition*. pp. 2423–2432 (2021)

9. Hammernik, K., Klatzer, T., Kobler, E., Recht, M.P., Sodickson, D.K., Pock, T., Knoll, F.: Learning a variational network for reconstruction of accelerated MRI data. *Magnetic resonance in medicine* **79**(6), 3055–3071 (2018)
10. Han, Y., Sunwoo, L., Ye, J.C.: k-space deep learning for accelerated mri. *IEEE transactions on medical imaging* **39**(2), 377–386 (2019)
11. Huang, X., Belongie, S.: Arbitrary style transfer in real-time with adaptive instance normalization. In: *Proceedings of the IEEE International Conference on Computer Vision*. pp. 1501–1510 (2017)
12. Khan, S., Huh, J., Ye, J.C.: Switchable and tunable deep beamformer using adaptive instance normalization for medical ultrasound. *IEEE Transactions on Medical Imaging* (2021)
13. Knoll, F., Hammernik, K., Kobler, E., Pock, T., Recht, M.P., Sodickson, D.K.: Assessment of the generalization of learned image reconstruction and the potential for transfer learning. *Magnetic resonance in medicine* **81**(1), 116–128 (2019)
14. Knoll, F., Murrell, T., Sriram, A., Yakubova, N., Zbontar, J., Rabbat, M., Defazio, A., et al.: Advancing machine learning for MR image reconstruction with an open competition: Overview of the 2019 fastMRI challenge. *Magnetic resonance in medicine* **84**(6), 3054–3070 (2020)
15. Knoll, F., Zbontar, J., Sriram, A., Muckley, M.J., Bruno, M., Defazio, A., et al.: fastMRI: A publicly available raw k-space and DICOM dataset of knee images for accelerated mr image reconstruction using machine learning. *Radiology: Artificial Intelligence* **2**(1), e190007 (2020)
16. Korkmaz, Y., Dar, S.U., Yurt, M., Özbey, M., Cukur, T.: Unsupervised mri reconstruction via zero-shot learned adversarial transformers. *IEEE Transactions on Medical Imaging* (2022)
17. Liu, X., Wang, J., Liu, F., Zhou, S.K.: Universal undersampled mri reconstruction. In: *International Conference on Medical Image Computing and Computer-Assisted Intervention*. pp. 211–221. Springer (2021)
18. Liu, X., Wang, J., Sun, H., Chandra, S.S., Crozier, S., Liu, F.: On the regularization of feature fusion and mapping for fast mr multi-contrast imaging via iterative networks. *Magnetic resonance imaging* **77**, 159–168 (2021)
19. Qin, C., Schlemper, J., Caballero, J., Price, A.N., Hajnal, J.V., Rueckert, D.: Convolutional recurrent neural networks for dynamic MR image reconstruction. *IEEE transactions on medical imaging* **38**(1), 280–290 (2018)
20. Recht, M.P., Zbontar, J., Sodickson, D.K., Knoll, F., Yakubova, N., Sriram, A., Murrell, T., Defazio, A., et al.: Using deep learning to accelerate knee MRI at 3T: Results of an interchangeability study. *American Journal of Roentgenology* **215**(6), 1421–1429 (2020)
21. Schlemper, J., Caballero, J., Hajnal, J.V., Price, A.N., Rueckert, D.: A deep cascade of convolutional neural networks for dynamic MR image reconstruction. *IEEE transactions on Medical Imaging* **37**(2), 491–503 (2017)
22. Sriram, A., Zbontar, J., Murrell, T., Defazio, A., Zitnick, C.L., Yakubova, N., Knoll, F., Johnson, P.: End-to-end variational networks for accelerated MRI reconstruction. In: *International Conference on Medical Image Computing and Computer-Assisted Intervention*. pp. 64–73. Springer (2020)
23. Sriram, A., Zbontar, J., Murrell, T., Zitnick, C.L., Defazio, A., Sodickson, D.K.: GrappaNet: Combining parallel imaging with deep learning for multi-coil MRI reconstruction. In: *Proceedings of the IEEE/CVF Conference on Computer Vision and Pattern Recognition*. pp. 14315–14322 (2020)

24. Wang, S., Su, Z., Ying, L., Peng, X., Zhu, S., Liang, F., Feng, D., Liang, D.: Accelerating magnetic resonance imaging via deep learning. In: 2016 IEEE 13th International Symposium on Biomedical Imaging. pp. 514–517. IEEE (2016)
25. Wei, K., Aviles-Rivero, A., Liang, J., Fu, Y., Schönlieb, C.B., Huang, H.: Tuning-free plug-and-play proximal algorithm for inverse imaging problems. In: International Conference on Machine Learning. pp. 10158–10169. PMLR (2020)
26. Yang, G., Yu, S., Dong, H., Slabaugh, G., Dragotti, P.L., Ye, X., et al.: DAGAN: Deep de-aliasing generative adversarial networks for fast compressed sensing MRI reconstruction. *IEEE transactions on medical imaging* **37**(6), 1310–1321 (2017)
27. Yang, Y., Sun, J., Li, H., Xu, Z.: Deep ADMM-Net for compressive sensing MRI. In: Proceedings of the 30th international conference on neural information processing systems. pp. 10–18 (2016)
28. Zbontar, J., Knoll, F., Sriram, A., Murrell, T., Huang, Z., Muckley, M.J., et al.: fastMRI: An open dataset and benchmarks for accelerated MRI. arXiv preprint arXiv:1811.08839 (2018)
29. Zhou, B., Schlemper, J., Dey, N., Salehi, S.S.M., Liu, C., Duncan, J.S., Sofka, M.: Dsformer: A dual-domain self-supervised transformer for accelerated multi-contrast mri reconstruction. arXiv preprint arXiv:2201.10776 (2022)
30. Zhou, B., Zhou, S.K.: DuDoRNet: Learning a dual-domain recurrent network for fast MRI reconstruction with deep T1 prior. In: Proceedings of the IEEE/CVF Conference on Computer Vision and Pattern Recognition. pp. 4273–4282 (2020)
31. Zhou, S.K., Greenspan, H., Davatzikos, C., Duncan, J.S., Van Ginneken, B., Madabhushi, A., Prince, J.L., Rueckert, D., Summers, R.M.: A review of deep learning in medical imaging: Imaging traits, technology trends, case studies with progress highlights, and future promises. *Proceedings of the IEEE* (2021)
32. Zhou, S.K., Rueckert, D., Fichtinger, G.: Handbook of medical image computing and computer assisted intervention. Academic Press (2019)

5 Supplementary Materials

Table S2. The reconstruction results with true side information, randomly generated side information and wrong side information on $4\times$ accelerated brain images.

PSNR(dB)			SSIM(%)		
True	Random	Wrong	True	Random	Wrong
41.70	40.93	40.70	97.93	97.69	97.61

Table S3. The impact of side information on the reconstruction of $4\times$ accelerated brain images. c: contrast, v: view, s: source.

1 side information						2 side information					
PSNR(dB)			SSIM(%)			PSNR(dB)			SSIM(%)		
c	v	s	c	v	s	c+v	c+s	v+s	c+v	c+s	v+s
41.39	40.94	41.20	97.86	97.71	97.76	41.42	41.67	41.25	97.87	97.91	97.78